

pubs.acs.org/NanoLett Letter

Bright Telecom-Wavelength Single Photons Based on a Tapered Nanobeam

Chang-Min Lee, Mustafa Atabey Buyukkaya, Samuel Harper, Shahriar Aghaeimeibodi, Christopher J. K. Richardson, and Edo Waks*



ACCESS I

Cite This: Nano Lett. 2021, 21, 323-329



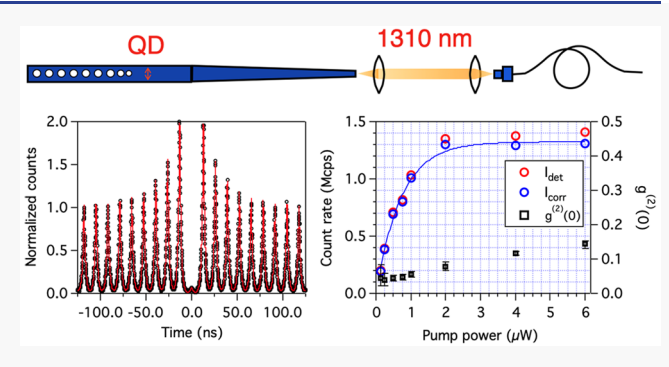
Article Recommendations

ABSTRACT: Telecom-wavelength single photons are essential components for long-distance quantum networks. However, bright

and pure single photon sources at telecom wavelengths remain challenging to achieve. Here, we demonstrate a bright telecomwavelength single photon source based on a tapered nanobeam containing InAs/InP quantum dots. The tapered nanobeam enables directional and Gaussian-like far-field emission of the quantum dots. As a result, using above-band excitation we obtain an end-to-end brightness of $4.1 \pm 0.1\%$ and first-lens brightness of $27.0 \pm 0.1\%$ at the ~1300 nm wavelength. Furthermore, we adopt quasi-resonant excitation to reduce both multiphoton emission and

decoherence from unwanted charge carriers. As a result, we achieve

III Metrics & More



Supporting Information

a coherence time of 523 ± 16 ps and postselected Hong-Ou-Mandel visibility of 0.91 ± 0.09 along with a comparable first-lens brightness of 21.0 ± 0.1%. These results represent a major step toward a practical fiber-based single photon source at telecom wavelengths for long-distance quantum networks.

KEYWORDS: single photon sources, quantum dots, telecom wavelength, two-photon interference

C ingle photons can serve as "flying qubits" to transfer quantum information over vast distances in extended quantum networks.1 Such photons must be bright and indistinguishable,^{2,3} and efficiently couple to optical fibers to enable efficient transmission.⁴ Semiconductor quantum dots have been extensively explored for these reasons, as their quantum emission properties demonstrate the necessary brightness and indistinguishability. 5-7 Furthermore, recent studies have reported quantum dots that emit at telecom wavelengths⁸⁻¹⁷ where photon transmission loss in optical fibers is minimized.¹⁸ However, these single photon sources must still efficiently couple with optical fibers in order to construct long-distance quantum networks.

Researchers have employed various photonic nanostructures to enhance the efficiency of single photon sources, such as nanowires, ^{19,20} planar photonic crystal waveguides, ⁸ and cavities. ^{17,21} Each nanostructure has different advantages in terms of collecting photons from the emitter, such as by coupling the single photons to the nanostructure's optical mode^{8,17,21} or enhancing the directional far-field emission.^{19,20} However, we need to improve the out-coupling efficiency of telecom-wavelength single photons into an objective lens and subsequent optical fiber in order to achieve single photon sources that are sufficient for long-distance quantum networks.

Toward this aim, we demonstrate a telecom-wavelength bright single photon source based on a tapered nanobeam. The

InP nanobeam contains InAs quantum dots that emit single photons at ~ 1300 nm (within the telecom O-band). We designed the tapered nanobeam to shape the far-field emission of the quantum dots to enable more efficient coupling of the emitted photons into an objective lens/optical fiber. Reflectivity measurements confirmed a high coupling efficiency of 60% into the objective lens at 1300 nm. Using above-band excitation, we obtained a first-lens brightness of $27.0 \pm 0.1\%$ and a record-high end-to-end brightness of 4.1 \pm 0.1%. We further confirmed the pure single photon emission using quasiresonant excitation and found $g^{(2)}(0) = 0.077 \pm 0.011$ at saturation power. The quasi-resonant excitation method also reduced the time jitter associated with carrier relaxation to the ground state of the quantum dot, which enhanced the coherence time to 523 ± 16 ps. This coherence time is 3.5 times larger compared to previously reported values using the same quantum dot wafer with above-band excitation. Due to the longer coherence time, we attained a high postselected visibility of 0.91 ± 0.09 with a similar first-lens brightness of

Received: Revised:

September 12, 2020 December 2, 2020 Published: December 18, 2020





 $21.0 \pm 0.1\%$. With this combined high brightness and postselected indistinguishability, these results take a step forward to a feasible telecom-wavelength single photon source for long-distance quantum networks.

Figure 1 shows a schematic of the tapered InP nanobeam containing InAs quantum dots, which served as the single

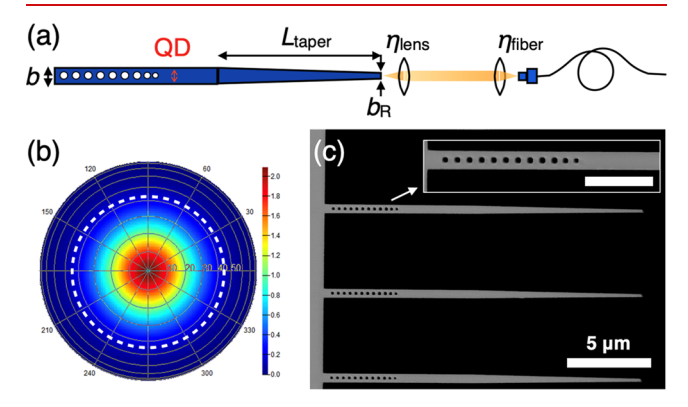


Figure 1. (a) Schematic of the tapered InP nanobeam containing InAs quantum dots. The emitted single photons are collected with an objective lens and subsequently coupled into an optical fiber. (b) Farfield emission profile at $L_{\rm taper}=10~\mu{\rm m},~b=400~{\rm nm},$ and $b_{\rm R}=150~{\rm nm}.$ 90% of the emission falls inside the white dashed circle, which represents the 0.66 numerical aperture of the objective lens. (c) Scanning electron micrograph of the tapered nanobeams. The inset shows a magnified image of the photonic crystal mirror at the nontapered end of the nanobeam. The scale bar in the inset is 2 $\mu{\rm m}$.

photon source. We designed the nanobeam so that emitted photons would be efficiently collected by an objective lens (numerical aperture of 0.66) and then coupled into an optical fiber. A photonic crystal mirror was added to the nontapered end of the nanobeam to ensure that all emitted photons moved toward the tapered end of the device. This tapered out-coupler spatially expands the nanobeam mode so that the single photon emission from the nanobeam becomes more directional ²²

We confirmed this directionality using finite-difference time-domain simulations (Lumerical FDTD solutions). Figure 1b shows the far-field pattern of the nanobeam mode at the linearly tapered end. We estimated the lens coupling efficiency ($\eta_{\rm lens}$) as a fraction of the far-field emission that falls within the numerical aperture of 0.66 (the white dashed circle in Figure 1b). To obtain a high lens-coupling efficiency, the tapered out-coupler should remain in the adiabatic condition to preserve the fundamental mode of the nanobeam. We investigated the taper length ($L_{\rm taper}$) dependence of the lens-coupling efficiency and found $L_{\rm taper}$ should be greater than 10 μ m to adiabatically enlarge the nanobeam mode to obtain high $\eta_{\rm lens}$ (see section 1 in the Supporting Information). At a taper length of 10 μ m, we achieved a lens coupling efficiency of 90% (Figure 1b).

Following the objective lens, the emitted photons must efficiently couple to an optical fiber. We estimated this coupling efficiency by calculating the overlap of the far-field pattern of the single photon emission with a Gaussian function. To do so, we fixed the taper length at $10 \mu m$, the height of the beam at 280 nm (i.e., the thickness of the epitaxial layer used in experiments), the nanobeam width (b) at 400 nm, and optimized the Gaussian overlap integral as a function of the tip width (b_R ; see section 2 in the Supporting Information). On the basis of the optimization, we used a tip

width of 150 nm to achieve a fiber coupling efficiency ($\eta_{\rm fiber}$) of 91%.

On the basis of these simulations, we fabricated the optimized designs of the InP nanobeams containing InAs quantum dots, which served as the single photon source. We grew the initial InAs/InP quantum dot wafer using molecular beam epitaxy and fabricated the tapered nanobeams with photonic crystal mirrors using e-beam lithography, reactive ion etching, and chemical wet etching (see section 3 in the Supporting Information). Then we used a home-built transfer print lithography system to suspend the nanobeams on the edge of a silicon wafer (Figure 1c; see section 3 in the Supporting Information for optical images of the transfer process). The suspended structure enabled us to pump the nanobeam with light directed from the optical fiber and objective lens down the nanobeam's length, and then collect the photons emitted directionally from the tip back through the same optical components (Figure 1a).

After fabricating the nanobeam structures, we determined their photon coupling efficiency with an objective lens. The lens coupling efficiency can be calculated by measuring the reflectivity of the nanobeam, which consists of the optics (e.g., mirrors and lenses) transmission in the system and the fiber coupling efficiency (see section 4 in the Supporting Information for details). Figure 2a demonstrates a typical

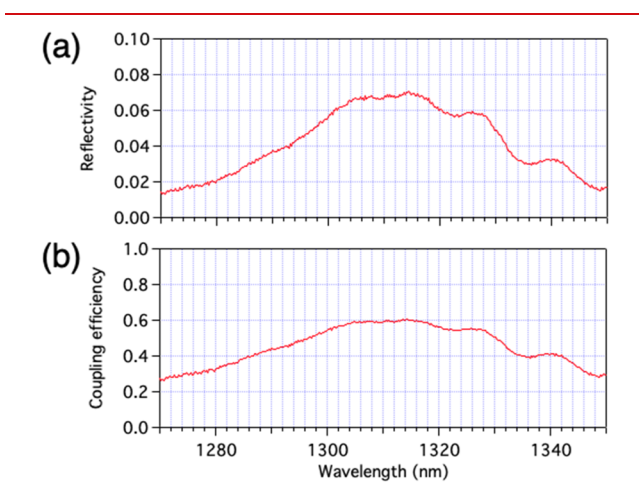


Figure 2. (a) Reflectivity spectrum measured from a nanobeam. (b) Coupling efficiency spectrum obtained from the reflectivity spectrum.

reflectivity spectrum of an individual nanobeam. On the basis of this spectrum, we calculated the lens coupling efficiency, as shown in Figure 2b. At \sim 1310 nm, we found the lens coupling efficiency was 60%. This value is a lower bound of the lens coupling efficiency as we assume perfect reflectance within the photonic crystal mirror (see section 4 in the Supporting Information). We attribute the discrepancy between this measured value and the simulated lens coupling efficiency (90%) to the below-unity reflectivity of the photonic crystal mirror, scattering loss from the surface roughness of the tapered out-coupler, and imperfect alignment of the nanobeam to the optic axis.

We then measured the photoluminescence spectrum of the nanobeam using above-band excitation at 780 nm as an initial assessment of the single photon source. For this and all subsequent measurements, we utilized a fiber-coupled photoluminescence measurement setup at 4 K with a Hanbury Brown and Twiss interferometer and a Hong-Ou-Mandel

interferometer (see section 5 in the Supporting Information). Figure 3a shows a photoluminescence spectrum of a

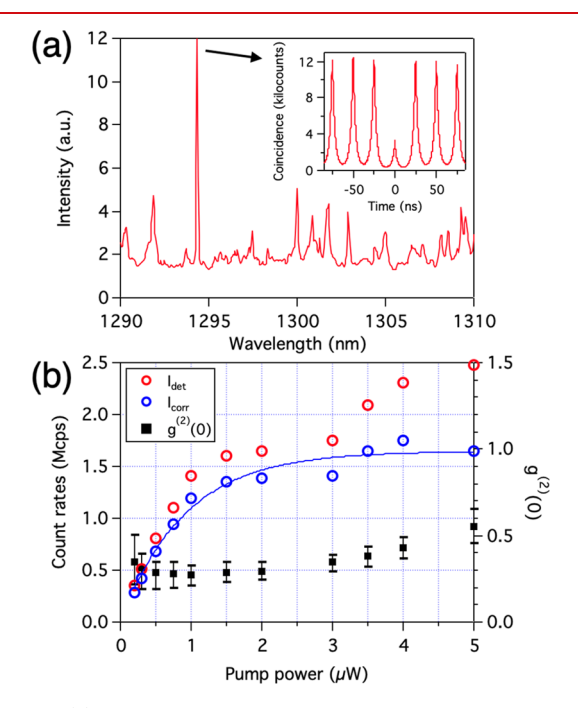


Figure 3. (a) Photoluminescence spectrum of a nanobeam produced using above-band excitation. The average pump power was 2 μ W. Inset: second-order autocorrelation histogram of the strong peak at 1294.3 nm. (b) Pump power dependence of the count rates and $g^{(2)}(0)$ from the peak at 1294.3 nm. The red circles are the detected count rates (I_{det}) and the blue circles are the count rates corrected with the $g^{(2)}(0)$ values (I_{corr}) . The blue line is a fitted curve to the I_{corr} data with fitting parameters of $I_{\text{sat}}=1.65\pm0.05$ Mcps and $P_{\text{sat}}=0.91$ μ W. The black dots are measured $g^{(2)}(0)$ values at each pump power.

nanobeam, in which we observed a strong and sharp peak at 1294.3 nm. To confirm single photon emission from the peak, we measured its second-order autocorrelation. From the histogram, we found clear antibunching with $g^{(2)}(0) = 0.26 \pm 0.09$ (Figure 3a, inset).

We measured the pump-power dependence of the single photon count rates and the second-order autocorrelation of the 1294.3 nm peak to estimate the brightness of the single photon source (Figure 3b). Since the above-band excitation gives rise to a significant amount of background emission from other quantum dots,²⁵ we observed $g^{(2)}(0) > 0.2$ for all pump powers. At the pump powers of $\bar{P} = 0.2 \ \mu \text{W}$ and $0.3 \ \mu \text{W}$, the $g^{(2)}(0)$ values are larger than those of higher pump powers, but they also have broader error bars as the fitting of the histogram becomes slightly off (section 6 in the Supporting Information). We corrected the detected count rates by multiplying by $\sqrt{1-g^2(0)}$ (blue circles in Figure 3b), which excluded unwanted background emission.²⁶ The corrected count rates showed a saturation behavior that we fit with a function of the form $I(P) = I_0 + I_{\text{sat}} \left(1 - \exp\left(\frac{P}{P_{\text{sat}}}\right) \right)^{2.6}$ From the fit, we found the maximum count rate to be $I_{\text{sat}} = 1.65 \pm 0.05$ Mcps (cps; counts per second) and a saturation power of P_{sat} = 0.91 μ W. The end-to-end brightness is defined by dividing I_{sat} by the repetition rate of the pumping laser (40 MHz), which gave us an end-to-end brightness of $4.1 \pm 0.1\%$.

On the basis of the obtained end-to-end brightness and detection efficiency of the setup, we can estimate the fiber-coupled brightness and first-lens brightness. The first-lens (fiber-coupled) brightness is defined as the single photon count rate at the first lens (collection fiber) divided by the repetition rate of the excitation laser. By dividing the end-to-end brightness of 4.1 \pm 0.1% by the 80% detection efficiency of the single photon detectors and 54% transmission of the fiber-type spectral filter, we obtained a fiber-coupled brightness of 9.5 \pm 0.1% (see section 7 in the Supporting Information for details of the photon budget). We also achieved a first-lens brightness of 27.0 \pm 0.1% by dividing the fiber-coupled brightness by a fiber coupling efficiency ($\eta_{\rm fiber}$) of 61% and optics transmission of 58%.

Although we attained this bright single photon source at telecom wavelength using above-band excitation, the single photon emission exhibits poor antibunching because we also pump other quantum dots in the nanobeam, which generates broad background emission. 25 As an alternative, quasi-resonant excitation can selectively excite an individual quantum dot, which minimizes the generation of unwanted charge carriers that occurs with above-band excitation.²⁷ The higher-order excited states of semiconductor quantum dots is typically separated by several tens of nanometers in wavelength from the s-shell. 15,16 To find the wavelength for the quasi-resonant excitation, we performed photoluminescence excitation measurements using a tunable continuous-wave laser (see section 8 in the Supporting Information). With the same nanobeam we used for the above-band excitation, we recorded the photoluminescence spectrum as we swept the wavelengths of the pumping laser. From this measurement we found an excited state of an individual quantum dot at 1269.2 nm, along with the position of the s-shell at 1312.8 nm (Figure S8).

After determining the excited state wavelength of a quantum dot, we performed photoluminescence measurements using laser pulses generated by an optical parametric oscillator pumped with a mode-locked Ti:sapphire laser operated at 76.5 MHz. By pumping with the pulsed laser at 1269.2 nm, we obtained a photoluminescence spectrum featuring a sharp peak at 1312.8 nm (Figure 4a). The quantum dot emission exhibited significantly reduced background compared to the spectrum obtained by above-band excitation (Figure 3a).

We then measured the second-order autocorrelation using the Hanbury-Brown and Twiss setup²⁸ to verify the pure single photon nature of the peak at 1312.8 nm. Figure 4b shows the autocorrelation histogram at a pump power of P =2.0 µW. To model the measured histogram, we fit the data using multiple two-sided exponentially decaying functions convolved with a Gaussian function representing a single photon detector response of 140 ps. For the first five timedelayed pulses, $g^{(2)}(t)$ reaches values significantly larger than 1, which indicates a blinking effect due to a metastable quantum dot state.²⁹ To normalize the plot, we divided the histogram counts by the mean peak height at time delays greater than 100 ns, where the blinking effect is averaged out and the photon statistics become Poissonian.²⁹ Similarly, by dividing the center peak area by the mean peak area at greater than 100 ns, we obtained a single photon purity of $g^{(2)}(0) = 0.077 \pm 0.011$. We attribute this low $g^{(2)}(0)$ value to the quasi-resonant excitation preventing other quantum dots in the nanobeam from being pumped, thereby reducing the background emission.

To determine the different brightness characteristics of the source, we measured the pump-power dependence of the

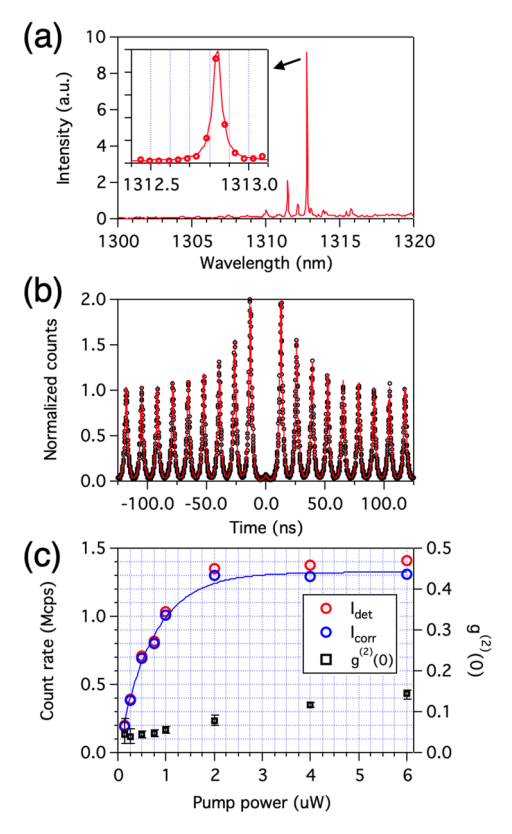


Figure 4. (a) Photoluminescence spectrum of the nanobeam using pulsed quasi-resonant excitation at 1269.2 nm (the same nanobeam previously used for above-band excitation measurements). Inset: zoomed in view of a peak at 1312.8 nm. The peak has a spectrometer-limited line width of 0.055 nm. (b) Second-order autocorrelation histogram of the peak at 1312.8 nm (black dots). The red curve is a fitted curve with two-sided exponentially decaying functions. (c) Pump-power dependence of the single photon count rates and $g^{(2)}(0)$. The red circles are the detected count rates (I_{det}) and the blue circles are the count rates corrected with the $g^{(2)}(0)$ values (I_{corr}) . The blue line is a fitted curve to theI_{corr} data with fitting parameters of $I_{\text{sat}} = 1.32 \pm 0.03$ Mcps and $P_{\text{sat}} = 0.72 \ \mu\text{W}$. The black squares are the measured $g^{(2)}(0)$ values.

single photon count rates and the second-order autocorrelation (Figure 4c). As in the above-band pumping measurements, we corrected the detected single photon count rates using the $g^{(2)}(0)$ values and fit the corrected count rates to obtain a saturation count rate of 1.32 ± 0.03 Mcps and a saturation power of P_{sat} = 0.72 μ W. Considering the detection efficiency of the detectors and the transmission of the components, we found a first-lens brightness of 21.0 \pm 0.2% (see section 9 in the Supporting Information). The discrepancy between this value and the first-lens brightness from the above-band excitation may derive from the different internal quantum efficiencies of the two quantum dots probed by the respective excitation schemes (see section 10 in the Supporting Information). We also measured the $g^{(2)}(0)$ values at different pump powers to confirm whether we can obtain pure single photons at high count rates (black squares in Figure 4c)). The $g^{(2)}(0)$ values remain below 0.1 until the saturation of the quantum dot, which suggest that the quasi-resonant excitation effectively suppresses the background emission.

To measure the indistinguishability of the single photons under quasi-resonant excitation, we conducted two-photon interference measurements using two unbalanced Mach—

Zehnder interferometers at both the excitation and collection paths (see section 5 in the Supporting Information). The unbalanced interferometer at the excitation path splits the pumping pulse into two separate pulses with a time delay (Δt) of 2.61 ns, which excite the quantum dot and generate two single photons with the same time delay. By coupling these single photons into the second unbalanced interferometer, they meet at the fiber beam splitter and interfere with each other, which allowed us to determine the single photon indistinguishability (for more details see section 5 in the Supporting Information).

Figure 5a shows the two-photon interference measurement, in which the interfering photons generated from the quasi-

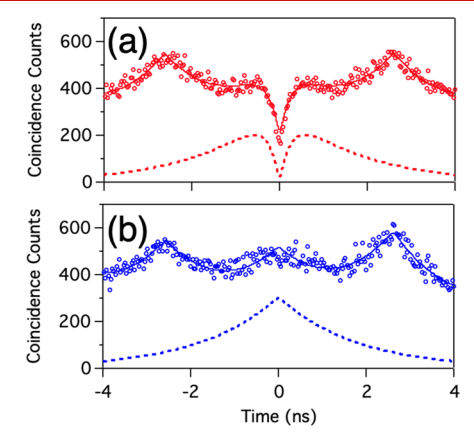


Figure 5. (a) Two-photon interference histogram at $P_{\rm sat}=0.72~\mu{\rm W}$ (red dots) with parallel-polarized input photons. The red curve is the fitted curve of the histogram. The red dashed line is the fitted curve of the center peak. (b) Two-photon interference histogram at $P_{\rm sat}=0.72~\mu{\rm W}$ (blue dots) with orthogonally polarized input photons. The blue curve is the fitted curve of the histogram, and the blue dashed line is the fitted curve of the center peak.

resonant excitation at $P_{\rm sat}=0.72~\mu{\rm W}$ demonstrate parallel (same) polarization (see section 5 of the Supporting Information). The center peak corresponds to the case in which the two single photons meet at the fiber beam splitter, and the side peaks originate from cases when one photon arrives at the beam splitter earlier than the second photon by the time delay $\Delta t=2.61$ ns. For an ideal source of indistinguishable photons, the peak at the zero-time delay should disappear due to the two-photon interference. ³⁰ In real experiments, the center peak appears but has a dip indicating that the coherence time is significantly shorter than the radiative lifetime. ³¹

We analyzed the histogram by fitting the center peak to the function $f(\tau) = \exp\left(-\frac{|\tau|}{\tau_c}\right) - \nu \cdot \exp\left(-\frac{2|\tau|}{\tau_c}\right)$, where τ_r is the spontaneous emission lifetime, τ_c is the coherence time of the quantum dot, and ν is a visibility fitting parameter. We fit the side peaks with two-sided exponentially decaying functions. All the peaks were convolved with a Gaussian function representing the instrumental response. From the fitting parameters of the center peak (red line in Figure 5a), we obtained a coherence time of $\tau_c = 523 \pm 16$ ps. Additionally, we observed a spontaneous emission lifetime of $\tau_r = 1.67 \pm 0.02$ ns. Note that quasi-resonant excitation improves the coherence time by more than 3-fold compared to the same quantum dot wafer excited by above-band laser. The coherence time is limited by a few mechanisms, such as time

jitter induced by nonradiative decay to the ground state exciton or charge noise caused by trapped charges around the quantum dots.³¹

We determined the indistinguishability of the single photons from the two-photon interference visibility, which is defined as $V=rac{A_{\perp}-A_{\parallel}}{A_{\perp}}$, where A_{\perp} (A_{\parallel}) is the center peak area of the twophoton interference histogram measured with input photons polarized in the orthogonal (parallel) configuration. We selected this definition over another common definition $V=1-rac{2A_{
m c}}{A_{
m l}+A_{
m r}}$, 33 where $A_{
m c}$ $(A_{
m l},\,A_{
m r})$ is the area of the center peak (the left peak, the right peak from the center, respectively), because the definition we used is less sensitive to the asymmetry of the side peaks. Figure 5b shows the twophoton interference histogram using photons in orthogonal polarization. The asymmetry of the side peaks in Figure 5b comes from a slight difference in the pumping pulse amplitudes and detector efficiencies.³⁴ On the basis of these results and the results in Figure 5a, we calculated a visibility of 0.20 ± 0.04 , which is consistent with the ratio of the lifetime to the coherence time $\frac{\tau_c}{2\tau_r} = 0.16 \pm 0.01$. Meanwhile, the postselected interference visibility of the single photons in the coherence time $au_{\rm c}$, defined as $V_{\rm ps} = \frac{g_{\rm L}^{(2)}(0) - g_{\rm ll}^{(2)}(0)}{g_{\rm l}^{(2)}(0)}$, was $V_{\rm ps} =$ 0.91 + 0.09.

The brightness and indistinguishability of telecom-wavelength single photon sources are key metrics for application in long-distance quantum networks. In both of these values, we demonstrate improvements from previous telecom-wavelength single photon sources. By employing the tapered nanobeam structure, our device shows an end-to-end brightness of 4.1 \pm 0.1%, which is an order of magnitude higher compared to previous works showing less than 1%.15-17 The first-lens brightness of $27.0 \pm 0.1\%$ is also significantly larger than most previous devices, except our earlier result demonstrating a firstlens brightness of 36% using photonic crystal cavities.¹⁷ However, compared to ref 17, which reported a $g^{(2)}(0)$ of close to 0.5, this work achieved a significantly improved single photon purity and coherence time by utilizing quasi-resonant excitation. To our knowledge, the coherence time of 523 \pm 16 ps that we observed is 2.5 times better than the best value³⁶ of reported telecom-wavelength single photon sources.

In summary, we have demonstrated a bright single photon source at telecom wavelengths based on a tapered InP nanobeam containing InAs quantum dots. We achieved a first-lens brightness of 27.0 ± 0.1% using above-band excitation, and $g^{(2)}(0) < 0.1$ and a coherence time of 523 \pm 16 ps using quasi-resonant excitation. Resonant pulsed excitation could further improve the indistinguishability by eliminating the time-jitter during the relaxation process and unwanted excess charges around the quantum dot. 30,31 We could further improve the indistinguishability of the single photons by coupling them to a cavity to enhance the spontaneous emission rate, 37,38 which would also increase the brightness of the single photon source by increasing the spontaneous emission coupling efficiency.³⁹ Another approach to elevate the brightness more would be to employ direct adiabatic fiber coupling techniques. 40 These results present a promising direction to achieve bright and indistinguishable telecom-wavelength photons, which could serve as essential

components for scalable quantum networks⁴¹ and photonic quantum computers.⁴²

ASSOCIATED CONTENT

Supporting Information

The Supporting Information is available free of charge at https://pubs.acs.org/doi/10.1021/acs.nanolett.0c03680.

Sample designs using numerical simulation, optical microscopy and SEM images of sample fabrication, optical measurement setup, analyses on the source brightness and PL measurement setup, analyses on the autocorrelations, PL spectra, tables of brightness parameters, and schematic images of polarizations (PDF)

AUTHOR INFORMATION

Corresponding Author

Edo Waks — Department of Electrical and Computer
Engineering and Institute for Research in Electronics and
Applied Physics, University of Maryland, College Park,
Maryland 20742, United States; Joint Quantum Institute,
University of Maryland and the National Institute of
Standards and Technology, College Park, Maryland 20742,
United States; orcid.org/0000-0003-0299-0784;
Email: edowaks@umd.edu

Authors

Chang-Min Lee – Department of Electrical and Computer Engineering and Institute for Research in Electronics and Applied Physics, University of Maryland, College Park, Maryland 20742, United States

Mustafa Atabey Buyukkaya — Department of Electrical and Computer Engineering and Institute for Research in Electronics and Applied Physics, University of Maryland, College Park, Maryland 20742, United States

Samuel Harper – Department of Electrical and Computer Engineering and Institute for Research in Electronics and Applied Physics, University of Maryland, College Park, Maryland 20742, United States

Shahriar Aghaeimeibodi — Department of Electrical and Computer Engineering and Institute for Research in Electronics and Applied Physics, University of Maryland, College Park, Maryland 20742, United States; Occid.org/0000-0002-9920-493X

Christopher J. K. Richardson – Laboratory for Physical Sciences, University of Maryland, College Park, Maryland 20740, United States; Occid.org/0000-0001-8817-5347

Complete contact information is available at: https://pubs.acs.org/10.1021/acs.nanolett.0c03680

Author Contributions

C.-M.L. and E.W. conceived the experiments, analyzed the measurement data, and prepared the manuscript. C.-M.L. conducted numerical simulations, transfer printing, and optical measurements. M.A.B. contributed to sample fabrication. S.H. contributed to data analysis. S.A. contributed to optical measurement setup. C.J.K.R. provided samples grown by molecular beam epitaxy.

Notes

The authors declare no competing financial interest.

■ ACKNOWLEDGMENTS

The authors acknowledge support from the National Science Foundation (grant numbers OMA1936314), the Army Research Office (grant number W911NF1910378), the Office of Naval Research (grant number N00014172720 and N000142012551), The Center for Distributed Quantum Information at the University of Maryland and Army Research Laboratory, The Maryland-ARL Quantum Partnership, and the U.S. Department of Defense.

■ REFERENCES

- (1) Northup, T. E.; Blatt, R. Quantum Information Transfer Using Photons. *Nat. Photonics* **2014**, *8* (5), 356–363.
- (2) Senellart, P.; Solomon, G.; White, A. High-Performance Semiconductor Quantum-Dot Single-Photon Sources. *Nat. Nanotechnol.* **2017**, *12* (11), 1026–1039.
- (3) Lodahl, P. Quantum-Dot Based Photonic Quantum Networks. Quantum Sci. Technol. 2018, 3 (1), 013001.
- (4) Wehner, S.; Elkouss, D.; Hanson, R. Quantum Internet: a Vision for the Road Ahead. *Science* **2018**, *362* (6412), No. eaam9288.
- (5) Somaschi, N.; Giesz, V.; De Santis, L.; Loredo, J. C.; Almeida, M. P.; Hornecker, G.; Portalupi, S. L.; Grange, T.; Antón, C.; Demory, J.; et al. Near-Optimal Single-Photon Sources in the Solid State. *Nat. Photonics* **2016**, *10* (5), 340–345.
- (6) Unsleber, S.; He, Y.-M.; Gerhardt, S.; Maier, S.; Lu, C.-Y.; Pan, J.-W.; Gregersen, N.; Kamp, M.; Schneider, C.; Höfling, S. Highly Indistinguishable on-Demand Resonance Fluorescence Photons From a Deterministic Quantum Dot Micropillar Device with 74% Extraction Efficiency. Opt. Express 2016, 24 (8), 8539–8546.
- (7) Wang, H.; He, Y.-M.; Chung, T. H.; Hu, H.; Yu, Y.; Chen, S.; Ding, X.; Chen, M. C.; Qin, J.; Yang, X.; et al. Towards Optimal Single-Photon Sources From Polarized Microcavities. *Nat. Photonics* **2019**, *13*, 770–775.
- (8) Hoang, T. B.; Beetz, J.; Lermer, M.; Midolo, L.; Kamp, M.; Höfling, S.; Fiore, A. Widely Tunable, Efficient on-Chip Single Photon Sources at Telecommunication Wavelengths. *Opt. Express* **2012**, 20 (19), 21758–21765.
- (9) Takemoto, K.; Nambu, Y.; Miyazawa, T.; Sakuma, Y.; Yamamoto, T.; Yorozu, S.; Arakawa, Y. Quantum Key Distribution Over 120Km Using Ultrahigh Purity Single-Photon Source and Superconducting Single-Photon Detectors. Sci. Rep. 2015, 5, 14383.
- (10) Müller, T.; Skiba-Szymanska, J.; Krysa, A. B.; Huwer, J.; Felle, M.; Anderson, M.; Stevenson, R. M.; Heffernan, J.; Ritchie, D. A.; Shields, A. J. A Quantum Light-Emitting Diode for the Standard Telecom Window Around 1,550Nm. *Nat. Commun.* **2018**, *9* (1), 862.
- (11) Lee, C.-M.; Buyukkaya, M. A.; Aghaeimeibodi, S.; Karasahin, A.; Richardson, C. J. K.; Waks, E. A Fiber-Integrated Nanobeam Single Photon Source Emitting at Telecom Wavelengths. *Appl. Phys. Lett.* **2019**, *114* (17), 171101.
- (12) Benyoucef, M.; Yacob, M.; Reithmaier, J. P.; Kettler, J.; Michler, P. Telecom-Wavelength (1.5Mm) Single-Photon Emission From InP-Based Quantum Dots. *Appl. Phys. Lett.* **2013**, *103* (16), 162101.
- (13) Al-Khuzheyri, R.; Dada, A. C.; Huwer, J.; Santana, T. S.; Skiba-Szymanska, J.; Felle, M.; Ward, M. B.; Stevenson, R. M.; Farrer, I.; Tanner, M. G.; et al. Resonance Fluorescence From a Telecom-Wavelength Quantum Dot. *Appl. Phys. Lett.* **2016**, *109* (16), 163104.
- (14) Nawrath, C.; Olbrich, F.; Paul, M.; Portalupi, S. L.; Jetter, M.; Michler, P. Coherence and Indistinguishability of Highly Pure Single Photons From Non-Resonantly and Resonantly Excited Telecom C-Band Quantum Dots. *Appl. Phys. Lett.* **2019**, *115* (2), 023103.
- (15) Dusanowski, Ł.; Holewa, P.; Maryński, A.; Musiał, A.; Heuser, T.; Srocka, N.; Quandt, D.; Strittmatter, A.; Rodt, S.; Misiewicz, J.; et al. Triggered High-Purity Telecom-Wavelength Single-Photon Generation From P-Shell-Driven InGaAs/GaAs Quantum Dot. Opt. Express 2017, 25 (25), 31122–31129.

- (16) Musial, A.; Zolnacz, K.; Srocka, N.; Kravets, O.; Große, J.; Olszewski, J.; Poturaj, K.; Wojcik, G.; Mergo, P.; Dybka, K.; et al. Plug&Play Fibre-Coupled 73 kHz Single-Photon Source Operating in the Telecom O-Band. 2019, 1912.10351v1. arXiv.org. https://arxiv.org/abs/1912.10351v1 (Dec 21, 2019).
- (17) Kim, J.-H.; Cai, T.; Richardson, C. J. K.; Leavitt, R. P.; Waks, E. Two-Photon Interference From a Bright Single-Photon Source at Telecom Wavelengths. *Optica* **2016**, *3* (6), 577–584.
- (18) Keiser, G. In *Optical Fiber Communications*, 3rd ed.; Proakis, J. G., Ed.; Wiley Online Library: Hoboken, NJ, USA, 2003.
- (19) Haffouz, S.; Zeuner, K. D.; Dalacu, D.; Poole, P. J.; Lapointe, J.; Poitras, D.; Mnaymneh, K.; Wu, X.; Couillard, M.; Korkusinski, M.; et al. Bright Single InAsP Quantum Dots at Telecom Wavelengths in Position-Controlled InP Nanowires: the Role of the Photonic Waveguide. *Nano Lett.* **2018**, *18* (5), 3047–3052.
- (20) Jaffal, A.; Redjem, W.; Regreny, P.; Nguyen, H. S.; Cueff, S.; Letartre, X.; Patriarche, G.; Rousseau, E.; Cassabois, G.; Gendry, M.; et al. InAs Quantum Dot in a Needlelike Tapered InP Nanowire: a Telecom Band Single Photon Source Monolithically Grown on Silicon. *Nanoscale* **2019**, *11* (45), 21847–21855.
- (21) Kors, A.; Fuchs, K.; Yacob, M.; Reithmaier, J. P.; Benyoucef, M. Telecom Wavelength Emitting Single Quantum Dots Coupled to InP-Based Photonic Crystal Microcavities. *Appl. Phys. Lett.* **2017**, *110* (3), 031101–031106.
- (22) Claudon, J.; Bleuse, J.; Malik, N. S.; Bazin, M.; Jaffrennou, P.; Gregersen, N.; Sauvan, C.; Lalanne, P.; Gérard, J.-M. A Highly Efficient Single-Photon Source Based on a Quantum Dot in a Photonic Nanowire. *Nat. Photonics* **2010**, *4* (3), 174–177.
- (23) Fu, Y.; Ye, T.; Tang, W.; Chu, T. Efficient Adiabatic Silicon-on-Insulator Waveguide Taper. *Photonics Res.* **2014**, 2 (3), A41–A44.
- (24) Bulgarini, G.; Reimer, M. E.; Bouwes Bavinck, M.; Jöns, K. D.; Dalacu, D.; Poole, P. J.; Bakkers, E. P. A. M.; Zwiller, V. Nanowire Waveguides Launching Single Photons in a Gaussian Mode for Ideal Fiber Coupling. *Nano Lett.* **2014**, *14* (7), 4102–4106.
- (25) Winger, M.; Volz, T.; Tarel, G.; Portolan, S.; Badolato, A.; Hennessy, K.; Hu, E.; Beveratos, A.; Finley, J.; Savona, V.; et al. Explanation of Photon Correlations in the Far-Off-Resonance Optical Emission From a Quantum-Dot-Cavity System. *Phys. Rev. Lett.* **2009**, 103 (20), 207403.
- (26) Pelton, M.; Santori, C.; Vučković, J.; Zhang, B.; Solomon, G.; Plant, J.; Yamamoto, Y. Efficient Source of Single Photons: a Single Quantum Dot in a Micropost Microcavity. *Phys. Rev. Lett.* **2002**, 89 (23), 233602.
- (27) Gazzano, O.; de Vasconcellos, S. M.; Arnold, C. Bright Solid-State Sources of Indistinguishable Single Photons. *Nat. Commun.* **2013**, *4*, 1425.
- (28) Brown, R. H.; Twiss, R. Q. Correlation Between Photons in Two Coherent Beams of Light. *Nature* **1956**, *177* (4497), 27–29.
- (29) Santori, C.; Fattal, D.; Vučković, J.; Solomon, G. S.; Waks, E.; Yamamoto, Y. Submicrosecond Correlations in Photoluminescence From InAs Quantum Dots. *Phys. Rev. B: Condens. Matter Mater. Phys.* **2004**, *69* (20), 205324.
- (30) He, Y. M.; He, Y.; Wei, Y. J.; Wu, D.; Atatüre, M.; Schneider, C.; Höfling, S.; Kamp, M.; Lu, C.-Y.; Pan, J.-W. On-Demand Semiconductor Single-Photon Source with Near-Unity Indistinguishability. *Nat. Nanotechnol.* **2013**, *8*, 213.
- (31) Huber, T.; Predojević, A.; Föger, D.; Solomon, G.; Weihs, G. Optimal Excitation Conditions for Indistinguishable Photons From Quantum Dots. *New J. Phys.* **2015**, *17* (12), 123025.
- (32) Predojević, A.; Mitchell, M. W. Engineering the Atom-Photon Interaction; Springer, Cham, 2015; p 347.
- (33) Santori, C.; Fattal, D.; Vuckovic, J.; Solomon, G. S.; Yamamoto, Y. Indistinguishable Photons From a Single-Photon Device. *Nature* **2002**, *419* (6907), 594–597.
- (34) Huber, D.; Reindl, M.; Huo, Y.; Huang, H.; Wildmann, J. S.; Schmidt, O. G.; Rastelli, A.; Trotta, R. Highly Indistinguishable and Strongly Entangled Photons From Symmetric GaAs Quantum Dots. *Nat. Commun.* **2017**, *8* (1), 15506.

- (35) Bylander, J.; Robert-Philip, I.; Abram, I. Interference and Correlation of Two Independent Photons. *Eur. Phys. J. D* **2003**, 22 (2), 295–301.
- (36) Srocka, N.; Mrowiński, P.; Große, J.; Helversen von, M.; Heindel, T.; Rodt, S.; Reitzenstein, S. Deterministically Fabricated Quantum Dot Single-Photon Source Emitting Indistinguishable Photons in the Telecom O-Band. *Appl. Phys. Lett.* **2020**, *116* (23), 231104.
- (37) Englund, D.; Fattal, D.; Waks, E.; Solomon, G.; Zhang, B.; Nakaoka, T.; Arakawa, Y.; Yamamoto, Y.; Vučković, J. Controlling the Spontaneous Emission Rate of Single Quantum Dots in a Two-Dimensional Photonic Crystal. *Phys. Rev. Lett.* **2005**, *95* (1), 013904.
- (38) Wang, H.; Duan, Z. C.; Li, Y. H.; Chen, S.; Li, J. P.; He, Y. M.; Chen, M. C.; He, Y.; Ding, X.; Peng, C.-Z.; et al. Near-Transform-Limited Single Photons From an Efficient Solid-State Quantum Emitter. *Phys. Rev. Lett.* **2016**, *116* (21), 213601.
- (39) Pelton, M. Modified Spontaneous Emission in Nanophotonic Structures. *Nat. Photonics* **2015**, 9 (7), 427–435.
- (40) Tiecke, T. G.; Nayak, K. P.; Thompson, J. D.; Peyronel, T.; de Leon, N. P.; Vuletic, V.; Lukin, M. D. Efficient Fiber-Optical Interface for Nanophotonic Devices. *Optica* **2015**, *2* (2), 70–75.
- (41) Kimble, H. J. The Quantum Internet. *Nature* **2008**, 453 (7198), 1023–1030.
- (42) Wang, H.; Qin, J.; Ding, X.; Chen, M.-C.; Chen, S.; You, X.; He, Y.-M.; Jiang, X.; You, L.; Wang, Z.; et al. Boson Sampling with 20 Input Photons and a 60-Mode Interferometer in a 1014-Dimensional Hilbert Space. *Phys. Rev. Lett.* **2019**, 123 (25), 250503.